Photoelectron spectroscopy of the solvated anion clusters O−(Ar) n=1–26,34: Energetics and structure

Susan T. Arnold, Jay H. Hendricks, and Kit H. Bowen

Articles you may be interested in

Anion photoelectron spectroscopy of solvated transition state precursors
J. Chem. Phys. **119**, 872 (2003); 10.1063/1.1577331

Photoelectron spectroscopy of pyrazine anion clusters
J. Chem. Phys. **117**, 1589 (2002); 10.1063/1.1488923

Photoelectron spectroscopy of naphthalene cluster anions
J. Chem. Phys. **116**, 4477 (2002); 10.1063/1.1449869

Photoelectron spectroscopy of copper cyanide cluster anions: On the possibility of linear and ring structures
J. Chem. Phys. **113**, 1725 (2000); 10.1063/1.481974

Photoelectron spectroscopy of iodine anion solvated in water clusters
J. Chem. Phys. **95**, 9416 (1991); 10.1063/1.461172

Photoelectron spectroscopy of the solvated anion clusters O⁻(Ar)$_{n=1-26,34}$: Energetics and structure

Susan T. Arnold,[a] Jay H. Hendricks, and Kit H. Bowen[b]

Department of Chemistry, Johns Hopkins University, Baltimore, Maryland 21218

Negative ion photoelectron spectra of the solvated anion clusters O⁻(Ar)$_{n=1-26,34}$ have been recorded. Vertical detachment energies obtained from the cluster anion spectra were used to determine total as well as stepwise stabilization energies. An examination of these energetic values as a function of cluster size demonstrates that the first solvation shell closes at $n=12$. Furthermore, magic numbers in the energetic data and in the mass spectrum suggest O⁻(Ar)$_n$ clusters of sizes $n=12-34$ are structurally very similar to homogeneous rare gas clusters and follow a polyicosahedral packing pattern, implying O⁻(Ar)$_{12}$ has an icosahedral structure and O⁻(Ar)$_{18}$ has a double icosahedral structure. The solvated cluster anion photoelectron data were also analyzed using a generalized cluster size equation, which relates the cluster anion data to bulk parameters. The data for O⁻(Ar)$_{n\geq12}$ is well represented by the theoretical prediction and was therefore used to estimate several bulk parameters, including the photoemission threshold, the photoconductivity threshold, and the bulk solvation energy. © *1995 American Institute of Physics.*

I. INTRODUCTION

A wide variety of experimental and theoretical studies have been conducted on gas-phase solvated ion clusters over the past couple of decades with the aim of elucidating the properties of these isolated species and their relationship to condensed phase analogs.[1,2] Negative ion photoelectron spectroscopy has proven to be a particularly useful technique for examining the energetics of cluster anions. Previously, we have studied a variety of solvated anion clusters, including H⁻(NH₃)$_n$, NO⁻(N₂O)$_n$, NH₂⁻(NH₃)$_n$, NO⁻(Rg)$_n$, and NO⁻(H₂O)$_n$ (Refs. 3–7); Johnson *et al.* have also investigated such species including O₂⁻(H₂O), O₂⁻(N₂), and NO₂⁻(N₂O) (Refs. 8–10). Lineberger *et al.* have examined H⁻(H₂O) (Ref. 11); and Brauman *et al.* have studied solvated anions of the form ROHF⁻.[12–14] These early studies, however, were limited to solvated anion clusters containing a relatively small number of solvent molecules. More recently, this technique has been applied to the study of solvated anion systems containing substantially more solvent molecules ($n=15-60$). In particular, Cheshnovsky *et al.*[15,16] have reported photoelectron spectra of X⁻(H₂O)$_n$ (where X=F, Cl, Br, and I) and Neumark *et al.*[17] have reported photoelectron spectra of I⁻(CO₂)$_n$. By examining the energetics of anion solvation over a substantial size range, photoelectron spectra have provided important information on the nature of the solvation shell structure around the anion. These experimental advances have also sparked a number of new theoretical investigations concerning the energetics and structure of large solvated anion systems.[18–27]

Evidence for shell closings in solvated ion clusters had previously been demonstrated in several important mass spectrometric and spectroscopic studies. High-pressure mass spectrometric studies presented the first experimental evidence for solvation shells in gas-phase solvated ion clusters. Investigations by Castleman *et al.*,[1,2,28–31] Kebarle *et al.*,[32–34] Meot-ner *et al.*,[35,36] and Hiraoka *et al.*,[37–41] measured changes in enthalpies of association as a function of cluster size, from which the number of molecules in the first solvation shell was inferred. In more recent mass spectrometric studies, Castleman *et al.*[42–44] have seen evidence of clathrate cage structures for ions in clusters of polar solvent molecules. Evidence for solvation shells has also come from photodissociation studies of gas phase solvated ion clusters. These include studies by Lineberger *et al.*,[45,46] Lisy *et al.*,[47,48] Lee *et al.*,[49–51] and Miller *et al.*[52,53]

Here, our ongoing investigation of solvated anion clusters continues, as we report the photoelectron spectra of an extended series of O⁻(Ar)$_n$ clusters. This study is meant to complement both the recent experimental studies on solvated anion complexes containing more strongly interacting solvent molecules, as well as theoretical studies on these solvated anion clusters. Given the complex nature of the ion–solvent and solvent–solvent interactions inherent in the solvated anion systems recently studied by photoelectron spectroscopy, our study of O⁻(Ar)$_n$ with relatively simple ion–solvent and solvent–solvent interactions provides a benchmark for comparison. In O⁻(Ar)$_n$, the atomic solvents have no propensity for chemical interactions with each other and only a weak propensity for chemical interactions with the atomic ion.

In this paper, we present the negative ion photoelectron spectra of O⁻(Ar)$_n$ clusters for $n=1-26$ and 34. Total and stepwise cluster solvation energies obtained from the spectra are examined as a function of size, revealing the closing of the first solvation shell at O⁻(Ar)$_{12}$. The structures of the O⁻(Ar)$_n$ clusters are further explored by comparing the evolution of the solvation energies with the approximate cluster temperature and the mass spectral data. Together, the experimental data imply a polyicosahedral pattern of structures for O⁻(Ar)$_n$ cluster ions with $n\geq12$. Finally, the cluster anion
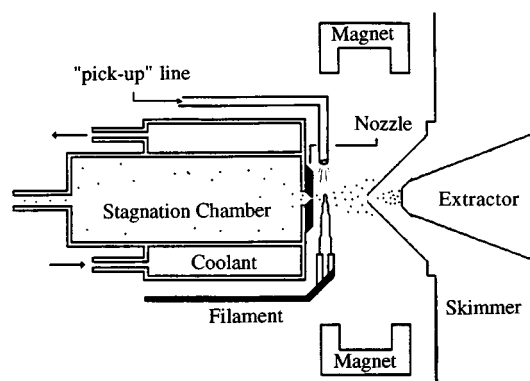

FIG. 1. A schematic diagram of the supersonic expansion cluster ion source used to generate O$^-$(Ar)$_n$ clusters. High pressure argon is expanded through a 12 μm diameter nozzle into high vacuum, while a small amount of N$_2$O is introduced through a "pick-up" line located near the expansion. Typical source conditions are as follows: stagnation pressure of 9 atm Ar, emission current of 5 mA, beam voltage of 500 V, extraction voltage of 700 V, and a filament bias voltage of 150 V (extraction and bias voltages are relative to the beam voltage).

FIG. 2. Typical mass spectrum of O$^-$(Ar)$_n$ cluster anions. "Magic numbers" are observed persistently at $n=12$, 18, 22, and 25, and usually at $n=15$.

photoelectron data were used to approximate the behavior of very large cluster anions, approaching bulk solvated anions.

II. EXPERIMENTAL METHOD

Negative ion photoelectron spectroscopy is conducted by crossing a mass-selected beam of negative ions with a fixed-frequency photon beam and energy analyzing the resultant photodetached electrons. The spectrometer has been described previously in detail.[54] A supersonic expansion ion source coupled with an additional gas "pick-up" line was used to generate the O$^-$(Ar)$_n$ cluster anions. This source is shown schematically in Fig. 1. Typically, 8–10 atm of argon was expanded through a 12 μm diameter nozzle, while a small flow of N$_2$O was introduced into the plasma through the secondary pick-up line located just beyond the nozzle. The source temperature was maintained at 196 K. A ThO$_2$/Ir filament was used for ionization, forming the primary anions O$^-$ and NO$^-$, which then clustered with the argon in the expansion yielding O$^-$(Ar)$_n$ and NO$^-$(Ar)$_n$ as the primary cluster anions. A predominantly axial magnetic field confined the plasma and enhanced cluster anion production. Cluster anions were extracted into the spectrometer and transported through a Wien velocity filter, where they were mass selected. The mass selected O$^-$(Ar)$_n$ cluster ion beam was then crossed with the photon beam of an argon ion laser operated intracavity at 488.0 or 457.9 nm. A small solid angle of the resulting photodetached electrons was energy analyzed using a hemispherical electron energy analyzer, with a typical resolution of 35 meV.

III. RESULTS AND ANALYSIS

A typical mass spectrum showing the distribution of O$^-$(Ar)$_n$ cluster anions produced by the ion source is presented in Fig. 2. Clear magic numbers were persistently observed in the mass spectrum at $n=12$, 18, 22, and 25, and usually at $n=15$.
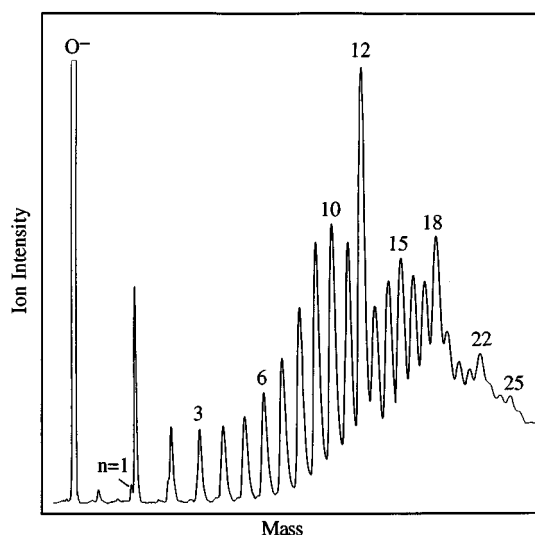
The negative ion photoelectron spectra of O$^-$(Ar)$_{n=1-26}$ are presented in Fig. 3, along with the spectrum of O$^-$, which was recorded before and after each cluster anion spectrum for calibration purposes. In each spectrum, the electron binding energy at the peak maximum is the cluster anion vertical detachment energy (VDE). The VDE of O$^-$ is 1.465 eV, while the electron affinity (E.A.) of O is slightly smaller 1.462 eV.[55] (Although the photoelectron spectrum of O$^-$ appears as a single, slightly broadened peak, it consists of six closely spaced transitions between the fine-structure states of O$^-$ and O.) The O$^-$ subion serves as the "chromophore" for photodetachment in the O$^-$(Ar)$_n$ cluster anions. Thus, the cluster anion spectra each closely resemble that of O$^-$, except for being broadened and shifted toward higher electron binding energy with increasing cluster size. The VDEs of O$^-$(Ar)$_{n=1-26,34}$ are reported in Table I.

The energetic information obtained from the photoelectron spectra can be rigorously related to cluster dissociation energies as follows:

$$E.A.[O(Ar)_n] = E.A.(O) + \sum_{m=0}^{n-1} D_0[O^-(Ar)_m \cdots Ar]$$

$$- \sum_{m=0}^{n-1} D_0[O(Ar)_m \cdots Ar], \tag{1}$$

where E.A. denotes the adiabatic electron affinity, $D_0[O^-(Ar)_m \cdots Ar]$ is the ion–neutral dissociation energy for the loss of a single Ar atom from the cluster, and $D_0[O(Ar)_m \cdots Ar]$ is the analogous neutral cluster dissociation energy for the loss of a single Ar atom. Since ion–solvent interaction energies generally exceed van der Waals bond strengths, it is evident from Eq. (1) that clustering can be expected to stabilize the excess electronic charge on a nega-
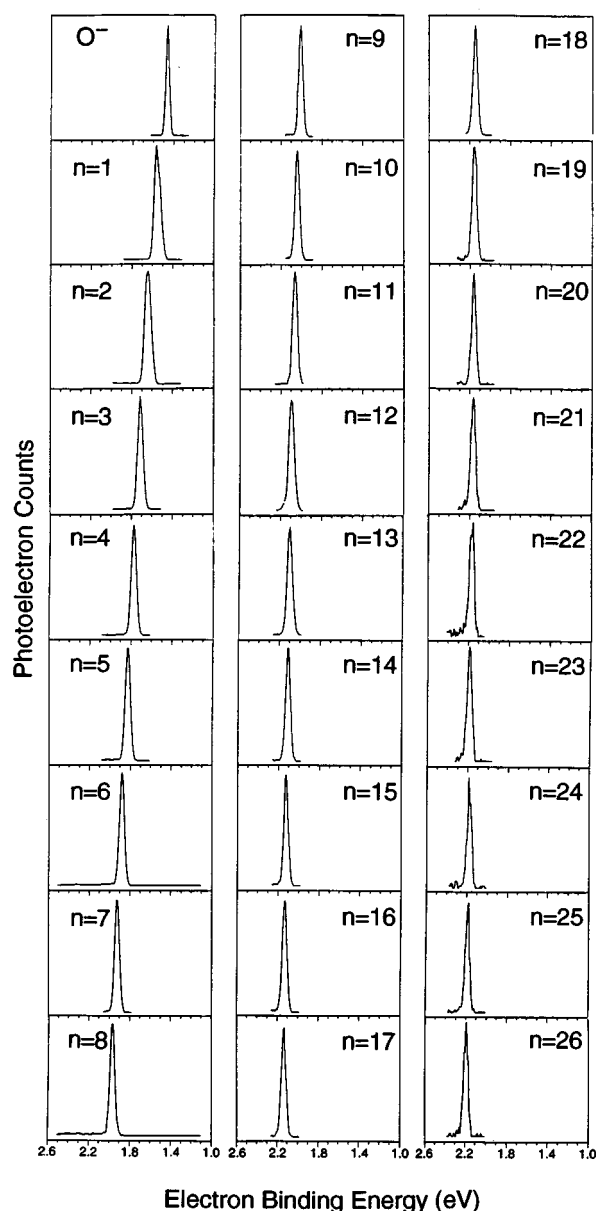
FIG. 3. Negative ion photoelectron spectra of $O^-(Ar)_{n=1-26}$ recorded with 2.54 eV photons. All the spectra closely resemble that of O^-, each containing a single peak which shifts to higher electron binding energy with increasing cluster size. The electron binding energy at the peak maximum is the VDE of the anion.

TABLE I. VDEs of $O^-(Ar)_{n=1-26,34}$. Total and stepwise stabilization energies were determined from the spectra as described in the text. All energies are in electron volts.

n	VDE	SE_{tot}	SE_{step}
1	1.562	0.097	0.097
2	1.648	0.183	0.086
3	1.717	0.252	0.069
4	1.778	0.313	0.061
5	1.828	0.363	0.050
6	1.881	0.416	0.053
7	1.926	0.461	0.045
8	1.967	0.502	0.041
9	2.008	0.543	0.041
10	2.039	0.574	0.031
11	2.058	0.593	0.019
12	2.091	0.626	0.033
13	2.098	0.633	0.007
14	2.105	0.640	0.007
15	2.122	0.657	0.017
16	2.127	0.662	0.005
17	2.133	0.668	0.006
18	2.143	0.678	0.010
19	2.149	0.684	0.006
20	2.155	0.690	0.006
21	2.159	0.694	0.004
22	2.165	0.700	0.006
23	2.171	0.706	0.006
24	2.177	0.712	0.006
25	2.184	0.719	0.007
26	2.191	0.726	0.007
34	2.243	0.778	

tive ion. It also follows from Eq. (1) that the relationship between the electron affinities of adjacent-sized clusters can be expressed as

$$E.A.[O(Ar)_n] - E.A.[O(Ar)_{n-1}]$$
$$= D_0[O^-(Ar)_{n-1} \cdots Ar] - D_0[O(Ar)_{n-1} \cdots Ar]. \quad (2)$$

Although the cluster E.A.'s are not explicitly reported in this work, they can be well approximated by the VDEs of the $O^-(Ar)_n$ cluster anions. Also, neutral–neutral interaction energies are significantly smaller than ion–solvent interaction energies, so their relatively minor contributions in Eqs. (1) and (2) may be neglected. Thus, the total anion solvent dis-

sociation (solvation) energy for a given cluster anion $SE_{tot}(n)$ may be approximated as the difference between the VDE of that species and the VDE of the subion

$$SE_{tot}(n) \approx VDE[O^-(Ar)_n] - VDE[O^-]. \quad (3)$$

Similarly, cluster ion–single solvent dissociation energies for $O^-(Ar)_n$ may be approximated by the difference between the VDEs of two adjacent-sized clusters. The cluster anion–single solvent dissociation energies are essentially stepwise solvation energies $SE_{step}(n)$ because they quantify the effect each individual argon solvent has on the overall stability of the $O^-(Ar)_n$ cluster

$$SE_{step}(n) \approx VDE[O^-(Ar)_n] - VDE[O^-(Ar)_{n-1}]. \quad (4)$$

Neglecting the weak bond dissociation energy of the neutral cluster is justified, as shown by examining the energetics of $O^-(Ar)_1$. For this particular cluster, the neutral dissociation energy $D_0(O\cdots Ar)$ is known (0.009 eV),[56–59] so the anion dissociation energy can be determined from Eq. (1). This leads to an anion dissociation energy of 0.106 eV, which is ~10% larger than the approximate value obtained from Eq. (3). The anion dissociation energy $[D_0(O^-\cdots Ar)]$ is greater than that of the neutral $[D_0(O\cdots Ar)]$ by an order of magnitude. Note that the anion dissociation energies obtained by measuring the spectral shifts represent a lower limit to the true value.

The total solvation energy for each $O^-(Ar)_n$ cluster as determined by Eq. (3) is listed in Table I and is shown as a function of cluster size in Fig. 4. Initially, SE_{tot} increases
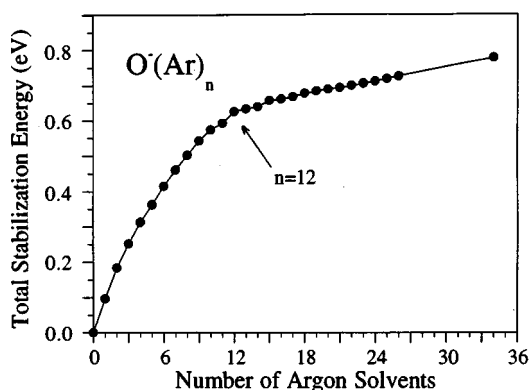
FIG. 4. Total anion solvent stabilization energy (SE_{tot}) of $O^-(Ar)_n$ plotted as a function of cluster size.

smoothly up to $n=12$, as the average stabilization energy per atom remains relatively constant. However, after $n=12$, the slope of the $SE_{tot}(n)$ plot changes abruptly, indicating that the average stabilization energy per atom decreases significantly for $n=13-34$.

The stepwise solvation energies for $O^-(Ar)_n$ obtained from Eq. (4) are also listed in Table I and are shown as a function of cluster size in Fig. 5. The interactions between O^- and the first few argon solvents are expected to be the strongest, while the stabilizing effect of each additional solvent should diminish as the cluster grows and the subion's localized charge interacts with a greater number of solvent atoms. In the absence of stabilizing effects, this should lead to a uniformly decreasing function of $SE_{step}(n)$ with increasing cluster size. The stepwise solvation energies do follow the expected generally decreasing trend. However, irregularities are observed at $n=6$, 12, 15, and 18, indicating that these particular clusters are stabilized by an additional effect. The largest single irregularity in the $SE_{step}(n)$ trend occurs at $n=12$, and this is followed by an abrupt drop in $SE_{step}(n)$ for $n=13$ and 14.
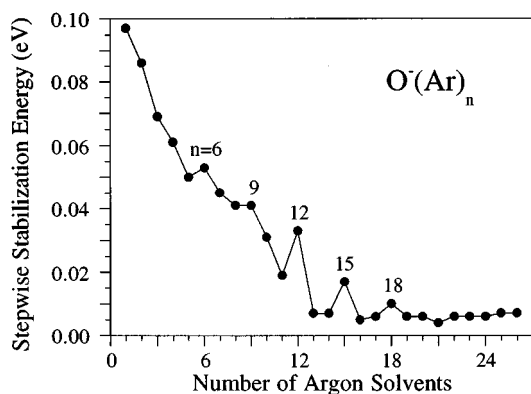

FIG. 5. Stepwise stabilization energies (SE_{step}) of $O^-(Ar)_n$ plotted as a function of cluster size. (Typical error bars for this data were ±5 meV or less.)
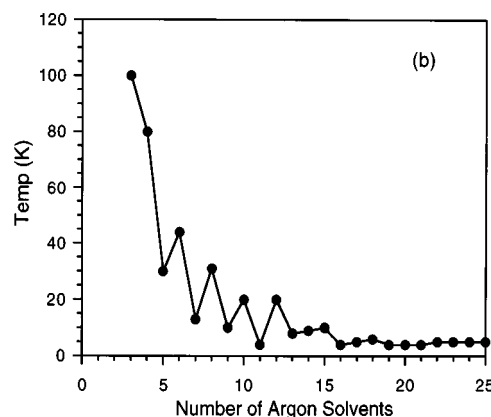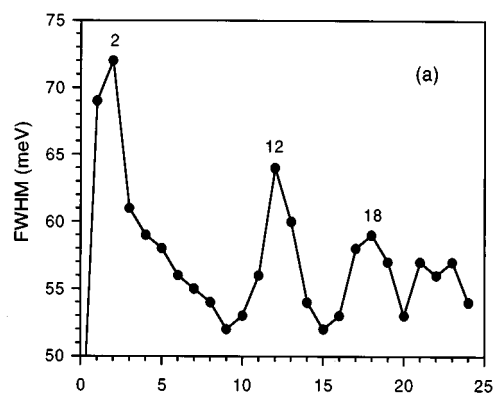

FIG. 6. (a) FWHM of the O^-Ar_n spectra plotted as a function of cluster size. (b) Calculated cluster internal temperatures plotted as a function of cluster size. Temperatures were calculated as described in the text.

In addition to the energetic information obtained from the photoelectron spectra, the spectra also yield information about the temperature of the clusters through the spectral broadening. For all of the solvated cluster anions we have studied to date, some degree of broadening is observed in the photoelectron spectra. Generally, the broadening increases with cluster size and with stronger ion–neutral interactions. The broadening is tracked as the peak full width at half-maximum (FWHM), and this is plotted for the $O^-(Ar)_n$ spectra as a function of cluster size in Fig. 6(a). The broadening in the $O^-(Ar)_n$ photoelectron spectra shows unusual behavior that is not a simple function of size. The broadening initially increases as expected. However, the spectra then become more narrow in the $n=3-10$ region and local maxima are observed again at $n=12$ and 18.

A number of mechanisms can contribute to the broadening in anion photoelectron spectra. (1) During photodetachment, there can be Franck–Condon overlap between the ground state of the anion and the repulsive portion of the neutral's potential energy surface due to a difference between the equilibrium structure of the anion and that of the neutral. (2) Spectral broadening can also result from photodetachment transitions between the ground state of the anion and vibrationally excited states of the neutral. This is manifested as broadening on the high electron binding energy side of the

origin peak. (3) Similarly, photodetachment transitions from excited weak-bond vibrations or other excited states of the anion to the various neutral states cause broadening especially on the low electron binding energy side of the origin peak.

The smallest $O^-(Ar)_n$ cluster spectra are broadened because of populated anion states and because of a geometry difference between the equilibrium structures of the anion and the neutral. (A detailed analysis of the spectral broadening in a series of rare gas oxide dimer anions will be the subject of a future publication.[60]) The most likely broadening mechanism for the larger cluster anions also involves the population of excited anion states, both vibrational and electronic, and the population of these states relates to the cluster ion's internal "temperature."

The temperature of these cluster anions can be estimated using a procedure outlined by Lisy et al.[47,48] The cluster ions are treated as an evaporative ensemble, where the initially formed clusters have excess internal energy that is dissipated by the successive loss of solvent monomers.[61,62] The evaporative cooling process is a unimolecular dissociation and can therefore be described by the classical Rice–Ramsperger–Kassel (RRK) model.[63] The rate constant is represented as

$$k_a(E) = A\left(1 - \frac{E_0}{E}\right)^{L-1}, \qquad (5)$$

where E is the internal energy, A is the pre-exponential factor and is taken to be equal to the vibrational frequency $(\sim 8 \times 10^{11}\ \mathrm{s}^{-1})$,[59] E_0 is the binding energy of a single solvent and is equal to the stepwise stabilization energies determined from the photoelectron spectra, and L is the number of normal modes. The result of such a treatment is the probability distribution $P_n(E,t)$ that a cluster ion contains internal energy E at time, t. Explicit expressions for $P_n(E,t)$ are given by Lisy et al.[47] From the probability distribution, average internal energies E_n are obtained and the cluster temperature is found by equating the average internal energy per vibrational mode to RT.

The calculated cluster ion internal temperatures are plotted in Fig. 6(b) as a function of cluster size. Generally, the internal temperature of the cluster anion is predicted to decrease with size. In most respects, this correlates with the decreasing FWHM observed in the photoelectron spectra beyond $n=2$ [see Fig. 6(a)], indicating that the spectral broadness is very probably related to the cluster ion's internal temperature. The local maxima in the FWHM plot at $n=12$ and 18 suggest those particular clusters have a higher internal temperature than their neighboring clusters, although the model itself does not predict such behavior.

The odd/even alternation observed in the temperature plot between $n=5-13$ is a consequence of the fact that the stepwise stabilization energy is not a smooth function. The most sensitive parameter in determining the average internal energy, and thus the cluster temperature, is the single argon binding energy, which has been directly measured in this experiment. It is therefore not surprising that irregularities in the stepwise stabilization energy plot are reflected in the predicted cluster temperature. As a final note, the calculated cluster ion internal temperature values plotted in Fig. 6(b)

are probably realistic approximations. Both theoretical and experimental estimates of the internal temperatures of relatively small argon clusters formed in supersonic expansions find values in the range predicted by the model.[64–67]

IV. INTERPRETATION

All the results presented above indicate that $n=12$ is a unique cluster in the series of $O^-(Ar)_n$ ions. This cluster anion corresponds to the most intense magic number in the mass spectrum, the size where the slope changes in the total solvation energy plot, the largest irregularity in the stepwise solvation energy plot, and a local maxima in the FWHM/temp plot. Not surprisingly, the exceptional stability of this species is partially a consequence of it having a unique geometry. In addition, however, this cluster ion marks the closing of the first solvation shell in the $O^-(Ar)_n$ series. The energetic data obtained from the photoelectron spectra clearly demonstrates the shell closing. The deviation in the $SE_{tot}(n)$ plot at $n=12$ indicates a fundamental change in how subsequent argon atoms interact with the cluster ion, and the decrease in the average stabilization energy at $n>12$ is a result of the additional argon atoms being effectively shielded from the subion. This is also clearly illustrated in the $SE_{step}(n)$ plot as a large irregularity at $n=12$. The energetic data also demonstrates that the O^- subion occupies an internal position within the argon cage rather than existing on the surface of the cluster. If the ion remained exposed on the surface of the cluster, the SE_{step} values for $n=12$ and $n=13$ would be comparable. However, there is a large difference in these two values and the small SE_{step} values for $n=13$ and 14 are consistent with the subion being shielded.

More specific structural information concerning the clusters is revealed through the mass spectral data. Magic numbers in mass spectra often signal the existence of particularly stable cluster ions and a number of mass spectral studies on small cations clustered with argon atoms suggest an icosahedral cage structure for the cluster ion size containing 12 solvent atoms.[68–75] The $O^-(Ar)_n$ mass spectrum has a magic number pattern very similar to that observed in homogeneous argon cluster cation mass spectra. In the size range of 10–35 atoms, the Ar_m^+ mass spectrum contains magic numbers at $m=13, 19, 23, 26, 29, 32,$ and $34,$[76] while magic numbers in the $O^-(Ar)_n$ mass spectrum occur at 13, 16, 19, 23, and 26 **total** atoms. (Total atom count includes the argon solvents plus the subion, i.e., $m=n+1$). The correlation between the mass spectra suggests these two systems have related structures and insight into the solvated anion cluster structures may come from an examination of the homogeneous cluster structure.

In the case of homogeneous Ar_m^+ clusters, several hard-sphere packing schemes have been examined to explain the magic numbers observed in the mass spectra. The dominant magic numbers at relatively large sizes correspond to stable structures in the Mackay full shell icosahedral sequence,[77] where an icosahedron of 12 atoms around a central atom is then surrounded by additional complete icosahedral shells. Each additional layer contains $(10n^2+2)$ atoms, leading to a sequence of magic numbers at $m=13, 55, 147, 309,$ etc. A number of investigators have also examined stable structures
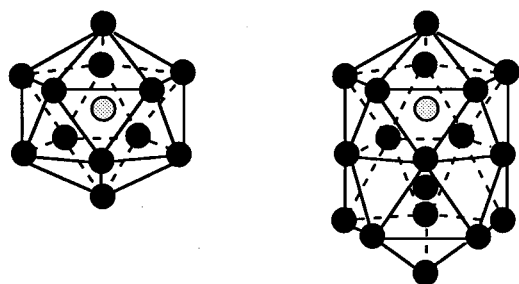
FIG. 7. Model structures for the magic number species $O^-(Ar)_{12}$, an icosahedron, and $O^-(Ar)_{18}$ a capped (double) icosahedron.

for the smaller homogeneous clusters, i.e., less than 50 atoms.[78–81] Hoare and Pal[78,79] examined minimum energy structures for clusters containing between six and 60 atoms based on three packing schemes—tetrahedral, pentagonal, and icosahedral sequences. The pentagonal sequence yields the lowest energy structures for $m = 6 - 20$, although all three sequences compete to give a variety of stable structures by $m \sim 23$. In the pentagonal packing sequence, several particularly stable geometries possess complete D_{5h} symmetry, including the pentagonal bipyramidal structure for the seven atom cluster, the icosahedral structure for the 13 atom cluster, and the capped (double) icosahedral structure for the 19 atom cluster. In contrast, the tetrahedral sequence predicts particularly stable structures for the four, eight, 14, and 26 atom clusters, while the icosahedral sequence begins with the 13 atom icosahedron and predicts particularly stable structures for the 33 and 45 atom clusters. Neither the tetrahedral nor the icosahedral sequences appear to explain the observed Ar_m^+ mass spectral distribution, although there is some correlation between the pentagonal sequence and the mass spectral magic numbers. However, a more thorough explanation for the magic numbers observed in the $m = 10 - 35$ region of the Ar_m^+ mass spectrum is the correlation of these magic numbers to the polyicosahedral sequence proposed by Farges et al.[80,81] This polyicosahedral scheme begins with the 13 atom icosahedron and then builds to the 19 atom double icosahedron. Additional atoms then add to the cluster in a manner that forms a number of interpenetrating icosahedral units. In addition to the 13 and 19 atom structures, the model predicts clusters containing 23, 26, 29, 32, and 34 atoms to be particularly stable, as structures are formed which contain several overlapping icosahedra. The stability of the polyicosahedral cluster series is expected to break down at $m \sim 35$ due to the stress occurring inside the icosahedral structure. The magic numbers predicted by this polyicosahedral growth sequence are in complete agreement with the magic numbers observed in this region of the Ar_m^+ mass spectrum. Furthermore, the correlation between the Ar_m^+ and $O^-(Ar)_n$ mass spectra suggests $O^-(Ar)_{12}$ is an icosahedron, $O^-(Ar)_{18}$ is a double icosahedron, and the larger $O^-(Ar)_n$ cluster ions have structures that contain a multiple number of overlapping icosahedra. Model structures for the magic number species $O^-(Ar)_{12}$ and $O^-(Ar)_{18}$ are shown in Fig. 7.

The possibility of the $O^-(Ar)_n$ cluster anions forming close-packed structures rather than the polyicosahedral structures discussed above has also been considered, especially for the 13 atom $O^-(Ar)_{12}$ cluster anion. The stability of homogeneous rare gas clusters in close-packed structures has been investigated by theory.[78–81] For clusters containing less than 50–100 atoms, the face-centered-cubic (fcc) or hexagonal-close-packed (hcp) type structures were found to be less stable than the corresponding noncrystalline structures. In particular, the cuboctahedral fcc type clusters containing 13 and 55 atoms were metastable and collapsed back to icosahedra. Thus, although the present study does not provide information that distinguishes between the two probable cage structures for $O^-(Ar)_{12}$, the icosahedral and the cuboctahedral structures, it seems very likely from the patterns observed in the experimental data along with the predicted relative stability of these structures that the $O^-(Ar)_{12}$ cluster does exist in an icosahedral form. (Recent experimental evidence of polyicosahedral packing for clusters in this size regime has also been reported by Parks et al.[82])

The structural implications of the mass spectral data are consistent with the interpretation of the photoelectron data presented previously. Analysis of the cluster anion energetics already indicated the special stability and uniqueness of the $O^-(Ar)_{12}$ cluster, including the fact that the first solvation shell closes at $n = 12$ and that the O^- subion is internalized at this point. The irregularity observed in the $SE_{step}(n)$ plot at $n = 18$ is also consistent with the mass spectral implications, namely that this is another very stable cluster. It is interesting, however, that the discontinuity at $n = 18$ is not more intense and that the additional stable polyicosahedral structures at $n = 22$ and 25 are not implicated in the $SE_{step}(n)$ plot. The reason for this is probably that, by this point, the stepwise solvation energy is comparable to an Ar–Ar interaction energy, and the difference between adjacent solvation energies has become smaller than we were able to measure. Nevertheless, the mass spectrum continues to illustrate these small and subtle differences, which suggests the polyicosahedral sequence continues in this size range. Concerning the irregularity in the $SE_{step}(n)$ plot at $n = 15$, we propose that it exists as a partially capped icosahedral structure, intermediate between the single and double icosahedral structures. The special characteristics of the $O^-(Ar)_{12}$ and $O^-(Ar)_{18}$ clusters were also highlighted in the FWHM/temp data, where both existed as local maxima. The symmetry and stability of these cluster anions allow them to exist at warmer temperatures than their neighboring clusters, although these clusters are still expected to be relatively cold.

For $O^-(Ar)_n$ clusters that contain an already filled first solvation shell, i.e., $n \geq 12$, the present study suggests the cluster anion structures resemble those of homogeneous rare gas clusters. Once the first layer of solvent molecules shields the subion, relatively weak induced-dipole interactions between rare gas atoms regulate the cluster structure. However, the nature of the cluster anion changes significantly for clusters smaller than $O^-(Ar)_{12}$. Because one of the components is an "unshielded" ion rather than a rare gas atom, a competition between the stronger ion–induced-dipole forces and the weaker induced-dipole interactions governs the cluster structure. Thus, the $O^-(Ar)_{n<12}$ structures do not necessarily
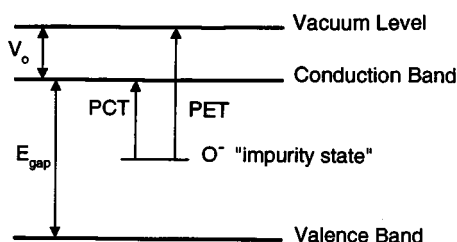
FIG. 8. A schematic energy level diagram of argon, showing the valance and the conduction bands with respect to the vacuum level. E_{gap} is the band gap of argon. V_0 is the electron affinity of the solvent and represents the edge of the conduction band relative to the vacuum level. The fully solvated anion O$^-$ is an impurity state in argon. PCT is the photoconductivity threshold for O$^-$ in argon and PET is the photoemission threshold.

resemble those of homogeneous rare gas clusters, and the structure of the smaller cluster ions in this series is more subtle. For example, the observed sequence of magic numbers seen in the SE$_{step}$(n) plot of O$^-$(Ar)$_n$ at $m=7$, 13, and 19 total atoms ($n=6$, 12, and 18) suggests that these cluster anions may follow a pentagonal packing pattern, which implies O$^-$(Ar)$_6$ exists as a pentagonal bipyramid, a structure which has no central atom. However, given the relative strength of the ion–neutral interactions in comparison to the neutral–neutral interactions, it is also possible that O$^-$ assumes a more central location in the O$^-$(Ar)$_6$ cluster, preferring a structure that maximizes the ion–neutral coordination number. Preliminary calculations by Kestner and Hall[83] indicate the minimum energy structure of O$^-$(Ar)$_6$ is an octahedral structure, with O$^-$ occupying the internalized position in the cluster, while the pentagonal bipyramidal structure is only slightly higher in energy. However, given a small but finite cluster temperature, both structures are expected to be populated. It is important to note that although several of the smaller cluster anions may have structures containing an internalized subion and thus display some of the "trappings" of solvation shell closings, such structures do not represent a true solvation shell closing. The term "solvation shell closing" not only pertains to geometry; it also pertains to energetics. The energetic data obtained from the photoelectron spectra, as shown in Figs. 4 and 5, indicate that 12 argon atoms are needed to completely fill the first solvation shell around an oxygen anion, thus maximizing the screening of the excess charge.

V. THE RELATIONSHIP TO BULK SOLVATED ANIONS

A number of investigators have examined the energetics of ion clustering in a stepwise manner, and this is the subject of several comprehensive review articles by Castleman *et al.*[1,2,28] It is of particular interest to obtain data that "bridges the gap" between the gaseous ion and the solvated ion in the condensed phase. In this context, it is noted that as the number of solvent atoms in the cluster becomes very large, the O$^-$(Ar)$_n$ system begins to model an O$^-$ "impurity" in an argon matrix. In Fig. 8, the valance and conduction bands of argon are shown with respect to the vacuum level, and the solvated anion "impurity state" is represented

as residing in the band gap. The difference between the vacuum level and the bottom of the conduction band is V_0 the electron affinity of the liquid. For argon, V_0 is $\sim$0.2 eV.[84] In the condensed phase, the minimum energy needed to promote an electron into the conduction band is the photoconductivity threshold (PCT), while the energy required to remove an electron from the solvated anion ground state into the vacuum level corresponds to the photoemission threshold (PET). On the molecular level, the vertical detachment energy (VDE) gives the energy required to vertically remove the excess electron from the cluster into vacuum. Thus, as the cluster ion size increases toward $n=\infty$, the VDE becomes a measure of the PET.

In an effort to relate the cluster data to bulk parameters, the energetic data obtained from the photoelectron spectra were analyzed in terms of a generalized cluster size equation, as formulated by Jortner,[85] which is meant to provide a quantitative description of the size dependence of cluster properties. The vertical ionization energy $I_v(n)$ of a solvated cluster anion $A^-(B)_n$ is given by the following:

$$I_v(n) = I_v(\infty) - A(m)^{-1/3}, \tag{6a}$$

or, in this context,

$$I_v(n) = I_v(\infty) - A(n+1)^{-1/3}. \tag{6b}$$

The slope is represented as

$$A = \frac{e^2}{2R_0}\left(1 - \frac{2}{\epsilon_0} + \frac{1}{\epsilon_\infty}\right), \tag{7}$$

where e is the fundamental charge, R_0 is the effective radius of the solvent atom or molecule (from the bulk density), ϵ_0 is the static dielectric constant of the solvent, and ϵ_∞ is the corresponding high frequency dielectric constant. For argon, R_0 is $\sim$2.06 Å, $\epsilon_0=1.538$, and $\epsilon_\infty=1.66$,[86] giving an expected value of 1.06 for the slope of this equation. As explained above, the value of the vertical ionization energy at infinite cluster size VDE(∞) closely approximates the bulk photoemission threshold (PET). The value of $I_v(\infty)=$PET has not been measured for this system, but it can be estimated as follows:

$$I_v(\infty) = I_v(\text{impurity}) + P^-(\infty), \tag{8}$$

where $I_v(\text{impurity})$ is the VDE of O$^-$, and $P^-(\infty)$ is the bulk polarization (solvation) energy associated with the anion as described by the Born equation

$$P^-(\infty) = \frac{e^2}{2R_i}\left(1 - \frac{1}{\epsilon_0}\right). \tag{9}$$

Here, R_i is taken to be the radius of the oxygen impurity $\sim$2.01 Å (from bulk density). The estimated bulk solvation energy is 1.25 eV, which leads to a $I_v(\infty)$ value of $\sim$2.71 eV. Thus, from the general cluster size equation [Eq. (6)] the O$^-$(Ar)$_n$ data in some size range are expected to be described by VDE(n)$=2.71-1.06(n+1)^{-1/3}$.

The energetics of O$^-$(Ar)$_n$ as n approaches infinite cluster size are examined by plotting the VDE as a function of $(n+1)^{-1/3}$. As shown in Fig. 9, the VDEs of O$^-$(Ar)$_n$ for $n\geq 12$, i.e., clusters after the first solvation shell closing, are linear with $(n+1)^{-1/3}$, and the data are described by the
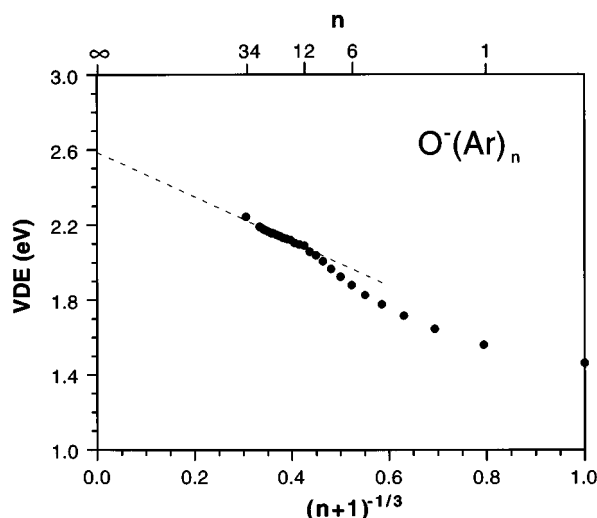
FIG. 9. VDEs of O^-Ar_n plotted as a function of $(n+1)^{-1/3}$. The VDEs of $n \geq 12$ (clusters beyond the first filled solvation shell) are linear with $(n+1)^{-1/3}$ and extrapolate to a VDE(∞) value of 2.6 eV.

equation $VDE(n) = 2.59 - 1.18(n+1)^{-1/3}$. Although the cluster size equation developed by Jortner is not expected to hold for small cluster sizes, the slope of the experimental line agrees very well with that predicted by the equation, and the extrapolated bulk vertical ionization value is also in reasonable agreement with the prediction. Agreement between both the slope and the intercept is not likely explained as an accidental empirical correlation and it suggests the cluster size equation as described above is applicable for $O^-(Ar)_n$ clusters where $n \geq 12$. Obviously, this model is not applicable for the smaller clusters in this study, as seen by their substantial deviation from linearity in Fig. 9. It should be noted that a general cluster size equation, based on similar principles, also explained the measured ionization potentials for rare gas clusters $n \geq 13$.[85]

The correlation with the experimental data suggests this model may be used to estimate a number of bulk values for anions solvated in rare gas matrices. From the extrapolation in Fig. 9, the bulk photoemission threshold (PET) is ~ 2.6 eV, while the photoconductivity threshold (PCT) can be inferred from the above discussion to be ~ 2.4 eV (PCT = PET$-V_0$). A refined value for the bulk solvation energy is 1.18 eV [$SE_{bulk} = PET - VDE(O^-)$]. Comparing the bulk solvation energy to the cluster solvation energy at the first shell closing implies that $\sim 55\%$ of the solvation energy is accounted for when the first solvation shell is filled. Using the extrapolation in Fig. 9 to obtain cluster solvation energies for $O^-(Ar)_{54}$ and $O^-(Ar)_{146}$, which are the expected second and third shell closings, demonstrates that only $75\% - 80\%$ of the total solvation energy is accounted for by this point. Compare this to the studies of Lee et al.,[31] who noted that for high dipole solvents such as water and ammonia, the ratio of the bulk solvation energy to the cluster solvation energy converged to near unity at relatively small cluster sizes. For hydrated anion clusters, $\sim 80\%$ of the bulk solvation energy had been reached by the addition of only five to six solvent molecules to the cluster. This is obviously a measure of how

strong the first interactions are between the ion and the solvent, and it is therefore not surprising that a large number of argon atoms are required to solvate an anion effectively, given the weak interactions involved.

VI. CONCLUSIONS

We have recorded the photoelectron spectra of $O^-(Ar)_{n=1-26,34}$ and have extracted total and sequential solvation energies from the spectra. An examination of these energetic values as a function of cluster size demonstrates that the first solvation shell closes at $n = 12$. Furthermore, magic numbers in the energetic data and in the mass spectrum suggest $O^-(Ar)_n$ clusters of sizes $n = 12 - 34$ are structurally very similar to homogeneous rare gas clusters and follow a polyicosahedral packing pattern. In particular, it is suggested that $O^-(Ar)_{12}$ has an icosahedral structure, while O^-Ar_{18} has a capped (double) icosahedral structure. Subtleties involving the structures of the smaller cluster anions $n < 12$ are due to a competition between the stronger ion–neutral forces and the weaker neutral–neutral interactions. The solvated cluster anion photoelectron data were also analyzed using a generalized cluster size equation, which relates the cluster anion data to bulk parameters. The data for $O^-(Ar)_{n \geq 12}$ is well represented by the theoretical prediction and was therefore used to estimate several bulk parameters, including the photoemission threshold, the photoconductivity threshold, and the bulk solvation energy.

ACKNOWLEDGMENTS

[1] T. D. Maerk and A. W. Castleman, Jr., *Advances in Atomic and Molecular Physics* (Academic, New York, 1985), Vol. 20, and references therein.

[2] A. W. Castleman, Jr. and R. G. Keesee, Chem. Rev. **86**, 589 (1986), and references therein.

[3] J. V. Coe, J. T. Snodgrass, C. B. Freidhoff, K. M. McHugh, and K. H. Bowen, J. Chem. Phys. **83**, 3169 (1985).

[4] J. V. Coe, J. T. Snodgrass, C. B. Freidhoff, K. M. McHugh, and K. H. Bowen, J. Chem. Phys. **87**, 4302 (1987).

[5] J. T. Snodgrass, J. V. Coe, C. B. Freidhoff, K. M. McHugh, and K. H. Bowen, Faraday Discuss. Chem. Soc. **86**, 241 (1988).

[6] K. H. Bowen and J. G. Eaton, in *The Structure of Small Molecules and Ions*, edited by R. Naaman and Z. Vager (Plenum, New York, 1988).

[7] J. G. Eaton, S. T. Arnold, and K. H. Bowen, Int. J. Mass Spectrom. Ion Processes **102**, 303 (1990).

[8] L. A. Posey, M. J. Deluca, and M. A. Johnson, Chem. Phys. Lett. **131**, 170 (1986).

[9] L. A. Posey, and M. A. Johnson, J. Chem. Phys. **88**, 5383 (1988).

[10] M. A. Johnson (private communication).

[11] T. M. Miller, D. G. Leopold, K. K. Murray, and W. C. Lineberger, Bull. Am. Phys. Soc. **30**, 880 (1985).

[12] C. R. Moylan, J. A. Dodd, and J. I. Brauman, Chem. Phys. Lett. **118**, 38 (1985).

[13] C. R. Moylan, J. A. Dodd, C. C. Han, and J. I. Brauman, J. Chem. Phys. **86**, 5350 (1987).

[14] D. M. Wetzel and J. I. Brauman, Chem. Rev. **87**, 607 (1987).

[15] G. Markovich, R. Giniger, M. Levin, and O. Cheshnovsky, J. Chem. Phys. **95**, 9416 (1991).

[16] G. Markovich, S. Pollack, R. Giniger, and O. Cheshnovsky, Z. Phys. D **26**, 98 (1993).

[17] D. W. Arnold, S. E. Bradforth, E. H. Kim, and D. M. Neumark, J. Chem. Phys. **97**, 9468 (1992).

[18] F. G. Amar, in *Physics and Chemistry of Small Clusters*, edited by P. Jena, B. K. Rao, and S. N. Khanna (Plenum, New York, 1987).

[19] C. Tsoo, D. A. Estrin, and S. J. Singer, J. Chem. Phys. **93**, 7187 (1990).

[20] L. Perera and M. Berkowitz, J. Chem. Phys. **95**, 1954 (1991).

[21] L. Perera and M. Berkowitz, J. Chem. Phys. **96**, 8288 (1992).

[22] L. Perera and M. Berkowitz, J. Chem. Phys. **99**, 4222 (1993).

[23] L. Perera and M. Berkowitz, J. Chem. Phys. **100**, 3085 (1994).

[24] I. Rips and J. Jortner, J. Chem. Phys. **97**, 536 (1992).

[25] J. E. Combariza, N. R. Kestner, and J. Jortner, J. Chem. Phys. **100**, 2851 (1994).

[26] R. L. Asher, D. A. Micha, and P. J. Brucat, J. Chem. Phys. **96**, 7683 (1992).

[27] T. Asado, K. Nishimoto, and K. Kitaura, J. Phys. Chem. **97**, 7724 (1993).

[28] A. W. Castleman, Jr., P. M. Holland, D. M. Lindsay, and K. I. Peterson, J. Am. Chem. Soc. **100**, 6039 (1978).

[29] I. N. Tang, M. S. Lian, and A. W. Castleman, Jr., J. Chem. Phys. **65**, 4022 (1976).

[30] R. G. Keesee, N. Lee, and A. W. Castleman, Jr., J. Chem. Phys. **73**, 2195 (1980).

[31] N. Lee, R. G. Keesee, and A. W. Castleman, Jr., J. Colloid Interface Sci. **75**, 555 (1980).

[32] W. R. Davidson and P. J. Kebarle, J. Am. Chem. Soc. **98**, 6125 (1976).

[33] P. J. Kebarle, Annu. Rev. Phys. Chem. **28**, 445 (1977).

[34] J. Sunner, K. Nishizawa, and P. Kebarle, J. Phys. Chem. **85**, 1814 (1981).

[35] M. Meot-ner, J. Am. Chem. Soc. **106**, 1265 (1984).

[36] M. Meot-ner and L. W. Sieck, Int. J. Mass Spectrom. Ion Processes **92**, 123 (1989).

[37] K. Hiraoka and T. Mori, J. Chem. Phys. **91**, 4821 (1989).

[38] K. Hiraoka and T. Mori, Chem. Phys. Lett. **154**, 139 (1989).

[39] K. Hiraoka and T. Mori, Chem. Phys. Lett. **157**, 467 (1989).

[40] K. Hiraoka and S. Yamabe, J. Chem. Phys. **95**, 6800 (1991).

[41] K. Hiraoka and S. Yamabe, J. Chem. Phys. **97**, 643 (1992).

[42] A. Selinger and A. W. Castleman, Jr., J. Phys. Chem. **95**, 8442 (1991).

[43] S. Wei, Z. Shi, and A. W. Castleman, Jr., J. Chem. Phys. **94**, 3268 (1991).

[44] X. Yang and A. W. Castleman, Jr., J. Phys. Chem. **94**, 8500 (1990).

[45] M. L. Alexander, N. E. Levinger, M. A. Johnson, D. R. Ray, and W. C. Lineberger, J. Chem. Phys. **88**, 6200 (1988).

[46] J. M. Papanikolas, J. R. Gord, N. E. Levinger, D. R. Ray, V. Vorsa, and W. C. Lineberger, J. Phys. Chem. **95**, 8028 (1991).

[47] J. A. Draves, Z. Luthey-Schulten, W. L. Liu, and J. M. Lisy, J. Chem. Phys. **93**, 4589 (1990).

[48] T. J. Selegue, N. Moe, J. A. Draves, and J. M. Lisy, J. Chem. Phys. **96**, 7268 (1992).

[49] M. Okumura, L. I. Yeh, and Y. T. Lee, J. Chem. Phys. **88**, 79 (1988).

[50] J. M. Price, M. W. Crofton, and Y. T. Lee, J. Chem. Phys. **91**, 2749 (1989).

[51] L. I. Yeh, M. Okumura, J. D. Myers, J. M. Price, and Y. T. Lee, J. Chem. Phys. **91**, 7319 (1989).

[52] L. F. Dimauro, M. Heaven, and T. A. Miller, Chem. Phys. Lett. **104**, 526 (1984).

[53] C. Y. Kung and T. A. Miller, J. Chem. Phys. **92**, 3297 (1990).

[54] J. V. Coe, J. T. Snodgrass, C. B. Freidhoff, K. M. McHugh, and K. H. Bowen, J. Chem. Phys. **84**, 618 (1986).

[55] C. Feigerle, Ph.D. thesis, University of Colorado, 1983.

[56] C. D. Cooper and M. Lichtenstein, Phys. Rev. **109**, 2026 (1958).

[57] M. F. Golde and B. A. Thrush, Chem. Phys. Lett. **29**, 486 (1974).

[58] V. Aquilanti, G. Liuti, F. Vecchio-Cattive, and G. G. Volpi, Faraday Discuss. Chem. Soc. **55**, 187 (1973).

[59] K. P. Huber and G. Herzberg, *Constants of Diatomic Molecules* (Van Nostrand–Reinhold, New York, 1979).

[60] J. H. Hendricks, H. L. de Clercq, and K. H. Bowen (unpublished results).

[61] C. E. Klots, J. Chem. Phys. **83**, 5854 (1985).

[62] C. E. Klots, J. Chem. Phys. **98**, 1110 (1993).

[63] P. J. Robinson and K. A. Holbrook, *Unimolecular Reactions* (Wiley, New York, 1972), Chap. 3.

[64] R. S. Berry, J. Jellinek, and G. Natanson, Phys. Rev. A **30**, 919 (1984).

[65] J. Jelinek, T. L. Beck, and R. S. Berry, J. Chem. Phys. **84**, 2783 (1986).

[66] J. Jelinek, T. L. Beck, and R. S. Berry, J. Chem. Phys. **87**, 545 (1987).

[67] J. Farges, M. F. de Feraudy, B. Raoult, and G. Torchet, Surf. Sci. **106**, 95 (1981).

[68] A. J. Stace, J. Am. Chem. Soc. **106**, 4380 (1984).

[69] A. J. Stace, Chem. Phys. Lett. **113**, 355 (1985).

[70] A. Ding, J. H. Futrell, R. A. Cassidy, L. Cordis, and J. Hesslich, Surf. Sci. **156**, 282 (1985).

[71] E. Holub-Krappe, G. Gantefor, G. Broker, and A. Ding, Z. Phys. D **10**, 319 (1988).

[72] Y. Ozaki and T. Fukuyama, Int. J. Mass Spectrom. Ion Processes **88**, 227 (1989).

[73] R. L. Whetten, K. E. Schriver, J. L. Persson, and M. Y. Hahn, J. Chem. Soc. Faraday Trans. **86**, 2375 (1990).

[74] P. R. Kemper, M. T. Hsu, and M. T. Bowers, J. Phys. Chem. **95**, 10600 (1991).

[75] S. R. Desai, C. S. Feigerle, and J. C. Miller, J. Chem. Phys. **97**, 1793 (1992).

[76] I. A. Harris, R. S. Kidwell, and J. A. Northby, Phys. Rev. Lett. **53**, 2390 (1984).

[77] A. L. Mackay, Acta Crystallogr. **15**, 916 (1962).

[78] M. R. Hoare and P. Pal, Adv. Phys. **20**, 161 (1971).

[79] M. R. Hoare and P. Pal, J. Cryst. Growth **17**, 77 (1972).

[80] J. Farges, M. F. de Feraudy, B. Raoult, and G. Torchet, Surf. Sci. **156**, 370 (1985).

[81] J. Farges, M. F. de Feraudy, B. Raoult, and G. Torchet, J. Chem. Phys. **78**, 5067 (1983).

[82] E. K. Parks, B. J. Winter, T. D. Klots, and S. J. Riley, J. Chem. Phys. **96**, 8267 (1992).

[83] N. R. Kestner and R. W. Hall (private communication, 1994).

[84] W. Werner F. Schmidt, in *Excess Electrons in Dielectric Media*, edited by C. Ferradini and J. P. Jay-Gerin (CRC, Boca Raton, FL, 1991), Chap. 5.

[85] J. Jortner, Z. Phys. D **24**, 247 (1992).

[86] *CRC Handbook of Chemistry and Physics*, edited by R. C. Weast, M. J. Astle, and W. H. Bayer (CRC, Boca Raton, FL, 1986), pp. E67, F164.